Dalton Transactions

An international journal of inorganic chemistry

Accepted Manuscript

This article can be cited before page numbers have been issued, to do this please use: C. Villa-Pérez, A. Zabala-Lekuona, I. J. Vitorica Yrezabal , J. M. Seco, J. Cepeda, G. A. Echeverría and D. B. Soria, *Dalton Trans.*, 2024, DOI: 10.1039/D3DT02359A.

ROYAL SOCIETY OF CHEMISTRY

rsc.li/dalton

View Article Online
DOI: 10.1039/D3DT02359A

ARTICLE

Spin Canting and Slow Magnetic Relaxation in Mononuclear Cobalt(II) Sulfadiazine Ternary Complexes

Received 00th January 20xx,
Accepted 00th January 20xx

DOI: 10.1039/x0xx00000x

Cristian Villa-Pérez,*[a] Andoni Zabala-Lekuona,*[b] Iñigo J. Vitorica-Yrezabal,[c] José Manuel Seco,[b] Javier Cepeda,[b] Gustavo Alberto Echeverría[d] and Delia Beatriz Soria*[a]

The monomeric [Co(SDZ)$_2$phen] (**1**) and [Co(SDZ)(bq)Cl] (**2**) complexes have been synthesized and characterized (SDZ = sulfadiazine, phen = 1,10-phenanthroline, and bq = 2,2'-biquinoline). X-ray diffraction studies indicate that the SDZ acts as a bidentate ligand coordinating through the sulfonamide and the pyrimidine N atoms in both compounds. In complex **1**, the coordination sphere consists of two SDZ ligands and a bis-chelating phen ligand, giving rise to a CoN_6 coordination sphere. On the other hand, **2** has a CoN_4Cl core, with two N-atoms from the SDZ and two from the bq ligand. Both compounds have been studied by dc and ac magnetometry and display slow magnetic relaxation under an optimum external dc field (1kOe) at low temperatures. Moreover, compound **2** displays long range magnetic ordering provided by a spin-canted antiferromagnetism, which has been characterized by further field-dependent magnetic susceptibility measurements, FC/ZFC curves, hysteresis loops and frequency-independent ac curves. The signs of the calculated *D* parameters, positive in **1** and negative in **2**, have been rationalized according to the two lowest-lying transitions occurring in the orbital energy diagrams derived from *ab initio* ligand field theory (AILFT). In a following attempt to emerge the possible hidden zero-field SMM behaviour, Ni(II)-based **3** and Co(II)-doped Ni(II)-based (with a Ni:Co ratio of 0.9:0.1) heterometallic compound $\mathbf{2_{Ni}}$ were synthesized.

Introduction

Single-molecule magnets (SMMs) are compounds that show slow relaxation of the magnetization and magnetic hysteresis below a certain temperature (T_B, blocking temperature). Slow magnetic relaxation behaviour is linked to an energy barrier (*U*) originated from large anisotropy (*D* or axial zero-field splitting, *zfs*, parameter for 3d ions) on ions with a high-spin ground-state (*S*).[1] The earliest efforts in the search of compounds with larger energy barriers were dedicated to the development of polynuclear complexes with large total spin by increasing the number of coupled paramagnetic centres. However, the control of the magnetic anisotropy axes in polynuclear systems is complicated and in many cases, the increase of *S* led to a significant diminution of the magnetic anisotropy with subsequent poor SMM properties.[2] In light of this, molecules with a single anisotropic paramagnetic centre possessing the essential requirements for observing slow magnetic relaxation were discovered and called Single-ion magnets (SIMs) or mononuclear SMMs.[3] After the discovery of Ln(III) based SIMs, a remarkable number of studies have been reported involving mononuclear 4f based materials.[4] However, 3d row transition metals are still of great interest in the field of molecular magnetism and, thus, several studies on different ions (Cr(II)/(III), Mn(III), Fe(I)/(II), Co(II) and Ni(I)/(II)) have been made during the last years.[5–21]. Although large energy barrier values have been observed in transition-metal based SIMs (as high as U_{eff} = 450 cm^{-1} for a Co(II) linear complex[18]), further studies are necessary in order to reach the final goal of operating temperatures that are closer to room temperature. In other words, open hysteresis loops at high temperatures.

Co(II)-based complexes are good candidates in the development of SMMs due to their large magnetic anisotropy, which comes from a strong contribution of first-order spin-orbit coupling to the total magnetic moment. The magnetic properties of these complexes are strongly influenced by the coordination environment provided by the ligands, and there is a great interest in developing complexes with coordination numbers as low as possible, due to their expected large magnetic anisotropy.[17] High coordination numbers are known to suppress the orbital contribution (*L*, orbital angular momentum) and subsequent magnetic anisotropy. Indeed, the ground-state could be appropriately described by the spin (*S*) term. When low coordination numbers are obtained, the d orbitals fall within narrower energy simulating 4f orbitals of lanthanide compounds. For instance, the current and previous

[a] CEQUINOR (CONICET, CCT – La Plata), Departamento de Química, Facultad de Ciencias Exactas, Universidad Nacional de la Plata, Bv. 120 nº 1465 (1900), La Plata, Argentina. E-mail cristianvilla@quimica.unlp.edu.ar; soria@quimica.unlp.edu.ar
[b] Departamento de Química Aplicada, Facultad de Química, Universidad del País Vasco/Euskal Herriko Unibertsitatea (UPV/EHU), Paseo Manuel Lardizabal nº3, 20018, Donostia, Spain. E-mail andoni.zabala@ehu.eus
[c] Departamento de Química Inorgánica, Facultad de Ciencias, Universidad de Granada, 18071, Granada, Spain.
[d] IFLP (CONICET, CCT – La Plata), Departamento de Física, Facultad de Ciencias Exactas, Universidad Nacional de la Plata, 47 y 115 (1900), La Plata, Argentina.
† Footnotes relating to the title and/or authors should appear here.
Electronic Supplementary Information (ESI) available: [details of any supplementary information available should be included here]. See DOI: 10.1039/x0xx00000x

records of the largest barriers to the reversal of the magnetization in transition metal complexes are two linear Co(II) complexes.[17,18] Nevertheless, it has been also proved that compounds with higher coordination numbers could have significant magnetic anisotropy. Several Co(II) single-ion magnets with coordination numbers ranging from 2 to 8 and with diverse geometries have been reported so far [17–20,22–27]. Hence, selecting the right ligands for the development of suitable ligand fields is fundamental, as they will modulate the magnetic anisotropy of the metal ion and, therefore, the potential SMM/SIM behaviour.

In this work, we report novel complexes that are derivatives of the sulfadiazine ligand, which is a widely used antibiotic in both human and veterinary medicine. In addition, it has several coordination modes that could lead to a wide variety of materials.[28] Note that we planned this research project as a continuation of a previously published work reported by some of us, in which two sulfadiazine six coordinated Co(II) complexes with the ancillary ligands 2,2'-bipyridine and 6-mehoxyquinoline were described.[22] Both compounds showed to be field-induced SMMs with U_{eff} values of 50.6 K (2,2'-bipyridine derivative) and 13.7 K (6-mehoxyquinoline derivative). In the present case, the heterocyclic compounds 1,10'-phenanthroline and 2,2'-biquinoline have been used as ancillary ligands. The former one could provide a similar structure to the one studied with 2,2'-bipyridine, while the later one was selected as a bulkier ligand with the aim of sterically hindering some coordinating positions and, thus, for obtaining lower coordinated compounds.

The present work covers the synthesis and characterization of three novel compounds, as well as the following experimental and theoretical magnetic study.

Experimental

Synthetic procedures

Chemicals. All chemicals were of reagent grade and were used as commercially obtained without any further purification.

Synthesis of [Co(SDZ)$_2$phen] (1). 25 mL of a methanolic solution containing NaSDZ (1 mmol) and 1,10-phenanthroline (0.5 mmol) was added dropwise to 25 mL of a $CoCl_2{\cdot}6H_2O$ solution (0.5 mmol, MeOH) under continuous stirring at room temperature. After 1 h the complex was filtered as an orange powder, and the filtrate was left for slow evaporation. After a few days, orange single crystals were recovered and used for the structural determination by XRD measurements. The elemental analysis (EA) gave the following results for $CoC_{32}H_{26}N_{10}O_4S_2$ (PM: 737.68): Experimental (calculated): C, 51.71 (52.10); H, 3.49 (3.55); N, 18.70 (18.99); S, 8.94 (8.68) %. The reaction yield was 87.6 %.

Synthesis of [TM(SDZ)(bq)Cl] (TM = Co for 2; TM = Ni for 3). 0.5 mmol of NaSDZ, 0.5 mmol of 2,2'-biquinoline, and 30 mL of an ethanol/methanol mixture (5:1) were placed in a two necked round bottom flask provided with a condenser and a dropping funnel. The system was heated to reflux and after the complete dissolution of the ligands, an ethanolic solution of the corresponding metal chloride (0.5 mmol, 10 mL) was dropwise added from the funnel. The reflux was maintained under continuous stirring for 1 h. During the reaction, the compound was obtained as green powder, which was hot filtered and washed with ethanol. The filtrate was preserved for slow evaporation and after a few days, green crystals were obtained and used in the structural determination in case of **2**. Single crystals for **3** were obtained by recrystallization in ethanol. The EA gave the following results for $CoC_{28}H_{21}N_6O_2SCl$ (PM: 599.96): Experimental (calculated): C, 56.09 (56.05); H, 3.34 (3.53); N, 13.65 (14.01); S, 5.31 (5.34) %; $NiC_{28}H_{21}N_6O_2SCl$ (PM: 599.72): Experimental (calculated): C, 56.17 (56.08); H, 3.31 (3.53); N, 13.84 (14.01); S, 5.41 (5.35) %. The reaction yields were 82.2 and 79.6 % for **2** and **3**, respectively.

Synthesis of [$Co_{0.1}Ni_{0.9}$(SDZ)(bq)Cl] (2_{Ni}). The synthesis of the doped compound $\mathbf{2_{Ni}}$ was carried out following the same procedure described for **2-3**, but using a 1:10 Co:Ni ratio. Note that this is a routinely employed method usually used to dilute transition metal and lanthanide based SMMs in diamagnetic Zn(II) and Y(III) matrices, respectively.[29,30] The phase purity of the material was confirmed by PXRD (Figure S2). The stoichiometry of the material was determined by ICP-MS, which confirmed the Co:Ni ratio of 1:9 in the material.

Physical measurements

Elemental analyses (C, H, N, S) were performed on a Leco CHNS-932 microanalyzer. Magnetic susceptibility measurements were carried out on polycrystalline samples of the complexes with a Quantum Design SQUID MPMS-7T susceptometer at applied magnetic fields indicated in the main text. The susceptibility data were corrected for the diamagnetism estimated from Pascal's Tables, the temperature-independent paramagnetism, and the magnetization of the sample holder. Alternating current measurements were performed on a physical property measurement System-Quantum Design model 6000 magnetometer under a 3.5 G ac field and frequencies ranging from 60 to 10000 Hz.

ICP-MS analysis

A sample of around 20 mg was attacked with concentrated HNO_3 in a closed vessel of PFA (Savillex®) and was heated at 100 °C for 24 hours. The solution was diluted (1:55000) for the determination of the analytes. All the masses were measured using a balance weighing with the accuracy ±0.0001 g to avoid volumetric dilution related errors. The analyses were carried out following a slightly modified previously reported protocol[31] in a Thermo Fisher XSeriesII quadrupole ICPMS. The calibration was made using a multielemental solution of 10 ppm (PerkinElmer with traceability to NIST standards). A rhodium based solution was used as an internal standard. Quality control solutions (QCS) were repeatedly measured to ensure the quality of the results.

X-ray Diffraction Data Collection and Structure Determination

Data for the complexes were recorded with a Rigaku-Oxford Gemini diffractometer equipped with an EOS CCD detector (for compounds **1** and **2**) or Bruker VENTURE area detector (for compound **3**), both of which are equipped with a graphite-monochromated Mo-Kα (λ =

0.71073 Å) radiation. X-ray diffraction intensities were collected (ω-scans with θ- and κ-offsets), integrated, and scaled with the CrysAlisPro[32] suite of programs. The unit-cell parameters were obtained by least-squares refinement (based on the angular settings for all collected reflections with intensities larger than seven times the standard deviation of measurement errors). Data were corrected empirically for absorption employing the multi-scan method implemented in CrysAlisPro. The structures were solved by direct methods with SHELXS-97,[33] and the molecular models were refined by the full-matrix least-squares procedure on F^2 with SHELXL-97.[34] All but the amino H-atoms were positioned stereochemically and refined with the riding model and their displacement parameter set equal to 1.2 times the equivalent isotropic displacement parameter of the bonded carbon atoms. On the other hand, the amino H-atoms were located in a difference Fourier map phased on the heavier atoms and refined with N–H and H···H distances restrained to target values of 0.86(1) and 1.49(1) Å, respectively, and their displacement parameters set equal to 1.5 times the equivalent isotropic displacement parameter of the corresponding nitrogen atom.

Crystal data and refinement results are summarized in Table S1. CCDC 2040162, 2040161 and 2309444 for **1**-**3**, respectively, contain the supplementary crystallographic data for this paper. These data can be obtained free of charge from The Cambridge Crystallographic Data Centre.

The X-ray powder diffraction (XRPD) patterns were measured over powdered samples (Figures S1-S2). For data acquisition, a Philips X'PERT powder diffractometer was used with Cu-Kα radiation (λ = 1.5418 Å) over the range 5 < 2θ < 50° with a step size of 0.026° and an acquisition time of 2.5 s per step at 25 °C.

Computational details

Gaussian 16 package[35] was employed for partially (hydrogen positions) optimizing the excerpts of all compounds taken from the X-ray structures. These calculations were performed with DFT using the UB3LYP functional[36] with the TZV basis set for the metal atoms,[37] and the 6-31G** basis set for the rest of non-metal atoms.[38] *Ab initio* calculations were implemented in ORCA (version 5.0.3)[39,40] to estimate *zfs* parameters on aforementioned models. These single point calculations were conducted with B3LYP functional[41,42] using def2-TZVP basis sets for all atoms and def2-QZVPP for the metal atoms, recontracted for zeroth-order regular approximation (ZORA) relativistic approximation.[43–46] RIJCOSX approximation with appropriate auxiliary basis sets (def2/J)[45] were employed for all calculations. Calculations with state-average complete active space self-consistent field (SA-CASSCF) method were performed incorporating the five d-orbitals and seven (for **1** and **2**) and eight electrons (for **3**). Ten quartets and forty doublets for the Co(II)-based compounds and ten triplets and ten singlets for the Ni(II)-based were included.[47] NEVPT2 calculations were performed on SA-CASSCF converged wave functions to take in account the dynamic correlation,[48] a strategy successfully used earlier to obtain accurate estimations of the *zfs* parameters.[47,49]

Results and discussion

The reaction between NaSDZ, an additional chelating ligand and $CoCl_2{\cdot}6H_2O$ in alcoholic solutions gives rise to two mononuclear compounds with variable coordination geometry. Hence, they both display distinct static and dynamic magnetic properties arising from either bulk or single ion in origin.

Structural description of compounds [Co(SDZ)$_2$phen] (1) and [Co(SDZ)(bq)Cl] (2)

Complexes **1** and **2** crystallize in the orthorhombic $Pac2_1$ and monoclinic $P2_1/n$ space groups, respectively, both with 4 molecules per unit cell. Note that the description of **3** has been omitted due to the fact that is isostructural to **2**. Figure 1 shows the coordination sphere of the Co(II) cations bonded to the ligands together with the used labels. In **1**, the Co(II) ion displays a CoN_6 coordination sphere, whereas **2** has a CoN_4Cl environment. The SHAPE software was used for the calculation of the degree of distortion of the coordination polyhedra with respect to ideal geometries.[50] The results revealed that the geometry around the metal in **1** is close in shape to an octahedron (TPR-6), while **2** is closer to a square pyramid (SPY-5) when compared with ideal six and five vertex polyhedra, respectively (see Tables S2 and S3 in the Supporting Information). Noteworthy, both coordination environments are far from ideal polyhedra according to the large SHAPE values.

The coordination geometry distortion can be evidenced by the bond distances and angles in the coordination spheres (see Table S4). For **1**, the coordination sphere around Co(II) ion consists of the phen nitrogen atoms at 2.102(7) and 2.113(5) Å and four N-atoms from two SDZ molecules at 2.106(4), 2.193(5), 2.276(5) and 2.094(5) Å, completing a distorted octahedral geometry. All the bonding angles deviate from the ideal values. For instance, both SDZ ligands bond to the metal ion through the sulfonamido and one pyrimidine nitrogen atoms establishing four-membered CoNCN' rings with N-Co-N' chelating angles of 60.88° and 62.48°. On the other hand, the phen ligand chelates the metal ion forming an angle of 78.41°.

In **2**, the cation is surrounded by a distorted square pyramidal environment. The equatorial positions are occupied by a chlorine atom at 2.2746(2) Å, two nitrogen atoms from an SDZ ligand (2.1166(2) and 2.1735(2) Å), and another one of the bq at 2.061(4) Å. The apical position of the pyramid is occupied by the N-atom of the second bq at 2.039(5) Å. The Co(II) is located 0.405 Å above the base of the distorted square pyramid. The angles in the pyramidal base are deviated from the ideal 90°, with values ranging from 61.87° (N16–Co–N17) to 99.43° (Cl1–Co–N16). Similarly, the angles between the base atoms and the apical N220 deviate from the ideal value with values as low as 79.67° (N21–Co–N220) and as high as 119.01° (N16–Co–N220).

View Article Online
DOI: 10.1039/D3DT02359A

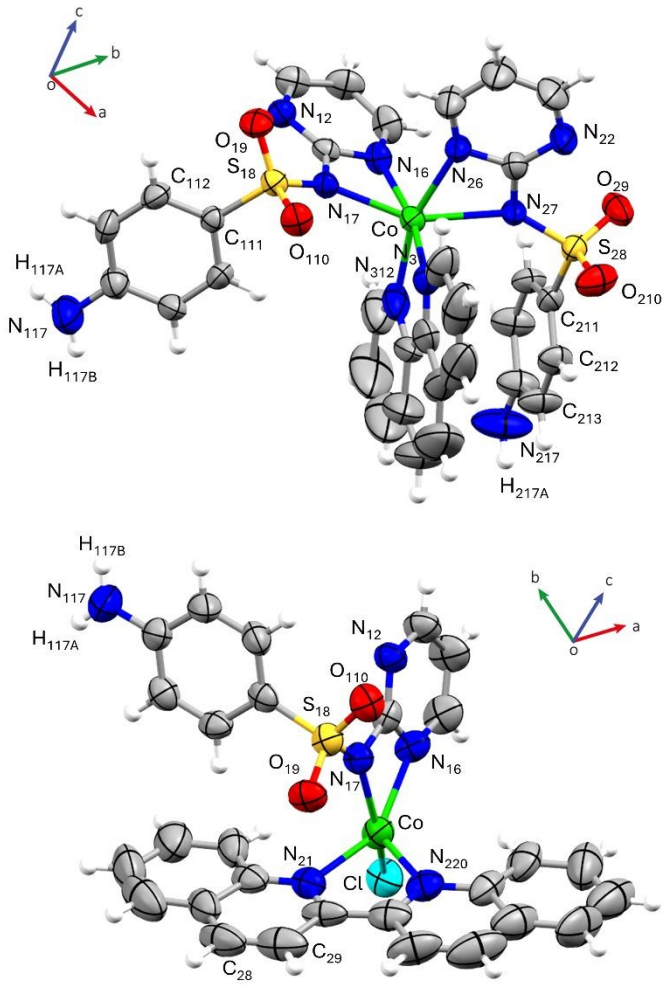

Figure 1. Crystal structure of the complexes **1** (top) and **2** (bottom). Co(II) ion, carbon, oxygen, nitrogen, sulphur, chloride and hydrogen atoms are shown by green, grey, red, blue, yellow, turquoise and white coloured Ortep ellipsoids (50% probability), respectively.

Furthermore, the crystal lattices are stabilized by the presence of several intermolecular hydrogen bonds (Table S5). In both complexes, the main intermolecular interactions, which stabilize the crystal structure, are the N-H···O hydrogen bonds connecting the anilinic SDZ nitrogen atom to the sulfonamide oxygen atoms generating an extended structural pattern. Besides, π···π intermolecular interactions also play an important role in the molecular packing of compound **2** as detailed below (Figure S3).

In **1**, the amino nitrogen and oxygen atoms of neighboring SDZ ligands, symmetry-related by the *c* and *a*-glide planes, are involved in four N-H···O hydrogen bonds forming a 3D N-H···O hydrogen bonding network that is spread along the three crystallographic directions (Figure 2). In addition, the supramolecular building is further stabilized by weaker C-H···N and C-H···O hydrogen bonds involving carbon atoms of the phenylamine group and pyrimidine nitrogen or sulfo oxygen atoms. Among all the intermolecular pathways, the shortest Co···Co distances are of 8.773(1) Å in **1**.

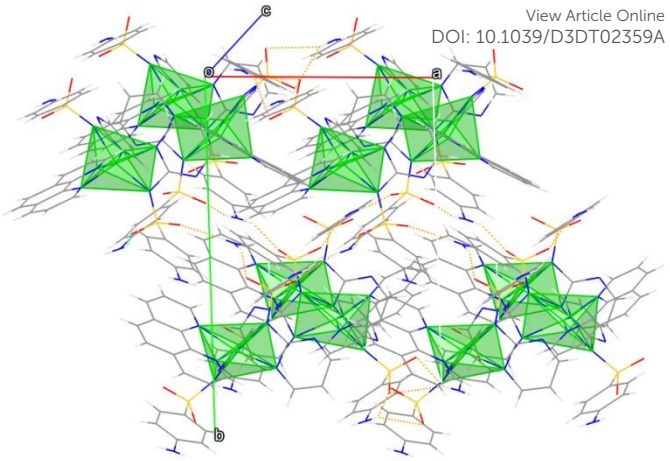

Figure 2. Extended unit cell content of compound **1** showing the 3D N-H···O hydrogen bonding network. Co(II) ion, carbon, oxygen, nitrogen and sulphur atoms are shown by green, grey, red, blue and yellow, respectively. For clarity, Co(II) coordination sphere and N-H···O hydrogen bonds are shown as polyhedra and orange dashed lines, respectively.

In **2**, the crystal building involves various types of interactions of variable nature and strength that set the neighbouring complexes at different distances between Co(II) centres. The main interaction between complexes is the formation of dimeric units through relatively strong π···π interactions (given the large overlap between central aromatic rings of bq ligands with C···C distances in the 3.5-3.7 Å range, see Table S6 for further details) and weaker C211-H211···Cl1 hydrogen bonds. This can be denoted as a centrosymmetric interaction pathway due to the presence of an inversion center that relates the stacked bq ligands at ca. 3.57 Å between centroids of interacting aromatic rings (see Figure S3). Interestingly, within these layers, bq ligands are packed in a fashion that resembles the herringbone packing of polycyclic aromatic hydrocarbons.[51,52] As a consequence, Co(II) ions of neighbouring complexes are placed at a distance of 7.2 Å, which is the shortest intermolecular pathway connecting the metal atoms. Moreover, each of the complexes of the centrosymmetric dimers establishes C-H···π interactions among SDZ ligands in addition to C221-H221···Cl1 (involving the aromatic bq carbon atom) weaker bonds to generate infinite arrays of complexes along the crystallographic *a* axis, by which complexes are separated with a Co···Co distance of 9.3 Å. As a result of both interaction pathways, 2D layers arranged along the (101) plane are formed (Figure 3). Note also that arrays of π···π stacked dimers are further linked with each other through additional π···π interactions between peripheral aromatic rings of bq ligands (Figure S3). At last, the 2D layers are further piled up one another along the crystallographic *b* axis in such a way that dimeric entities are displayed alternately with two alternative orientations with respect to the piling direction given that neighbouring layers are related by the glide *n* plane. Being as such, two inequivalent additional intermolecular pathways are observed between complexes pertaining to alternate layers: i) a first non-symmetric pathway involving the N117-H117A···O110 hydrogen bond established between the amino nitrogen and sulfonamido oxygen atoms of two neighboring SDZ (imposing a Co···Co distance of 11.2 Å); ii) a first non-symmetric pathway along the N117-H117B···Cl1 hydrogen bond established by the amino nitrogen atom of the SDZ ligand (imposing a Co···Co distance of 11.9 Å). Most importantly, these two patways share the absence of a symmetry

View Article Online
DOI: 10.1039/D3DT02359A

element operating between the involved complexes, but their relative orientation obeys to restrictions of the overall packing, in such a way that pyramidal environments are relatively twisted showing non-fully parallel nor anti-parallel orientations (to give an orientative measure, angles between Cu-N_{apical} vectors are of 59.3° and 82.3° for the non-symmetric pathways 1 and 2, respectively).

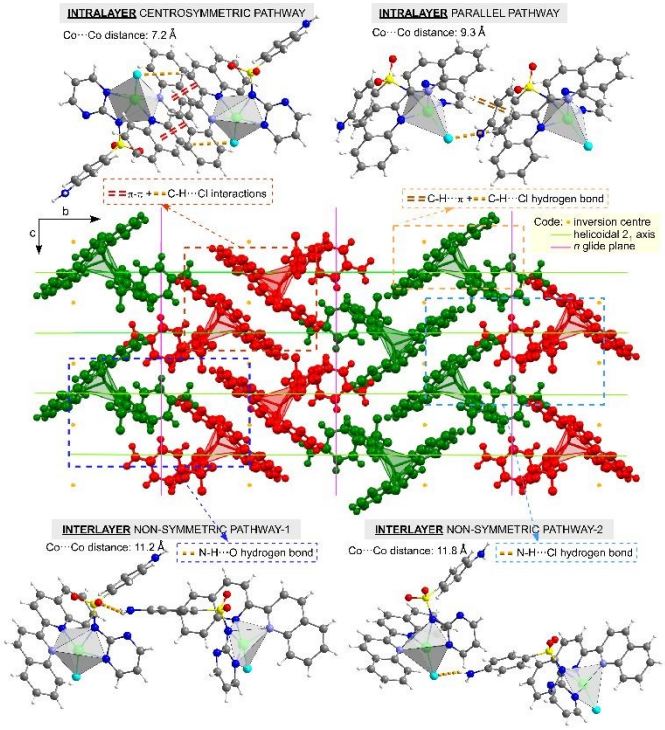

Figure 3. View of the crystal packing (central image) of compound **2** showing the symmetry elements along the [1 0 0] axis showing arrangement of complexes into 2D layers (in the *ac* plane) and their sequential arrangement (layers successively in green and red colours). The most relevant intermolecular interactions connecting the complexes with their respective Co···Co distances (to account for the plausible superexchange pathways) are also shown. Note that both π···π stackings between bq ligands and N-H···O / C-H···Cl / N-H···Cl hydrogen bonds between SDZ ligands are displayed.

Static magnetic properties

Variable-temperature (2-300 K) dependence of the magnetic susceptibility data was analysed over polycrystalline samples of **1-3** under a dc applied field of 1 kOe.

For **1**, the room temperature $\chi_M T$ product of 2.84 $cm^3 \cdot mol^{-1} \cdot K$ is significantly higher than the expected value for an octahedral Co(II) ion spin-only value (1.87 $cm^3 \cdot mol^{-1} \cdot K$ with g = 2.01), which suggests the presence of certain spin-orbit coupling (Figure 4). On cooling down, the $\chi_M T$ value remains almost constant before a final and more abrupt drop below 75 K reaching a minimum value of 1.68 $cm^3 \cdot mol^{-1} \cdot K$ at 2 K. This progressive decrease may be attributed to the first-order SOC effect as sizeable antiferromagnetic interactions have been ruled out in view of the long distances between spin carriers in the structure (the shortest interactions impose Co···Co distances of ca. 8.7 Å), and most importantly, the absence of remarkable π-π or hydrogen bonding interactions to mediate magnetic exchange. On account of the CoN_6 distorted octahedron present in compound **1**, the potential magnetic anisotropy usually present in those metal centres[53] was further corroborated by isothermal magnetization curves collected on the 2-5 K range (Figure 4, inset), as they do not reach the theoretical saturation for a $S = 3/2$ system (M_{sat} = 3.3 μ_B, with g = 2.2).

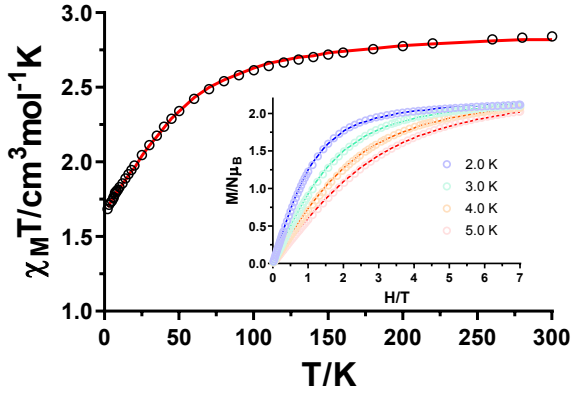

Figure 4. Variable-temperature dc magnetic susceptibility data for **1** collected under a 1 kOe applied dc field. Inset: the variable-field magnetization curves measured in the 2-5 K temperature range. The continuous lines in both plots represent fits to equation 2 using PHI program.

In order to evaluate the sign and magnitude of the *zfs* parameter, we simultaneously fitted both the susceptibility and magnetization data with the spin Hamiltonian shown in eq. 1 using the PHI program:[54]

$$\hat{H} = \boldsymbol{D}\left(\hat{S}_z^2 - {S(S+1)}/{3}\right) + \boldsymbol{E}\left(\hat{S}_x^2 - \hat{S}_y^2\right) + \boldsymbol{\mu_B H g \hat{S}} \qquad (1)$$

where S corresponds to the spin (S = 3/2), D and E account for the axial and rhombic magnetic anisotropies, respectively, and H is the applied magnetic field. The best fit provided the following set of parameters: D = +45.4 cm^{-1}, E/D = 0.33, g = 2.43, TIP = 2x10^{-4} and R = 3.8x10^{-4}. It must be noted that a similar result (with a slightly worse goodness of fit) could be obtained by changing the sign of D, which is not surprising given the large rhombicity estimated from the fitting (E/D = 0.33), which makes the sign of the main D parameter completely meaningless as largely discussed in several works.[55–57] *Ab initio* multireference calculations on a suitable model of **1** based on the X-ray coordinates overestimate the experimental result, but give a positive and almost axial *zfs* parameter (D = +70.1 cm^{-1} and E/D = 0.08, see Figure S6 and Table S7). According to the CASSCF calculation, the ground electronic state corresponds to the $(d_{xz})^2(d_{yz})^2(d_{xy})^1(d_{z^2})^1(d_{x^2-y^2})^1$ configuration (see Figure S4 and Tables S9-S10). These values, in line with those commonly observed for octahedral Co(II) ions,[47,58,59] although clearly overestimated with regard to experimental ones, confirm the suitability of the aforementioned fitting.

The temperature dependence of the $\chi_M T$ product for compound **2** notably differs from **1**, especially at the lowest temperatures (Figure 5). At room temperature, the $\chi_M T$ value of 3.41 $cm^3 \cdot mol^{-1} \cdot K$ is much higher than the expected spin-only value for a Co(II) ion. On cooling down, this value smoothly decreases reaching a minimum value of 3.17 $cm^3 \cdot mol^{-1} \cdot K$ at 46 K and then abruptly increases up to 6.34 $cm^3 \cdot mol^{-1} \cdot K$, describing a maximum at 11 K, eventually dropping to 2.26 $cm^3 \cdot mol^{-1} \cdot K$ at 2 K. This behaviour is indicative of a weak net ferromagnetic ordering in the compound, which is quite surprising in

View Article Online
DOI: 10.1039/D3DT02359A

view of the molecular nature of compound composed of isolated complexes. Nonetheless, the relatively short intermolecular Co···Co distances imposed by π··· π interactions between 2,2'-biquinoline ligands combined with other weak couplings along non-symmetric pathways in the structure seem to be responsible for the observed long-range ferromagnetic coupling (see Figure S5).

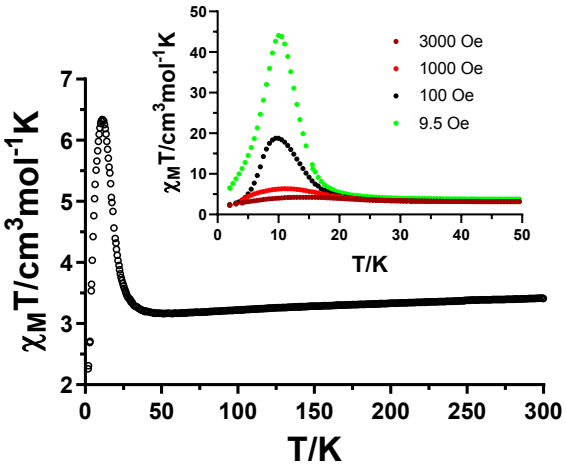

Figure 5. Variable-temperature dc magnetic susceptibility data for **2** collected under a 1 kOe applied dc field. Inset: $\chi_M T$ plots recorded under different external magnetic fields.

The occurrence of canted antiferromagnetism was further confirmed by several additional measurements. On the one hand, the susceptibility curves measured at variable fields reveal a strong field-dependence response (Figure 5, inset), which agrees with the usual behaviour observed for ferromagnetic compounds. Moreover, field-cooled (FC) and zero-field-cooled (ZFC) χ_M curves show a clear bifurcation at 11 K (Figure 6, top), which fits with the temperature at which frequency-independent maxima are observed in the ac dynamic magnetic measurements (*vide infra*). Lastly, isothermal magnetic hysteresis loops were recorded in the 2-5 K temperature range displaying a noticeable opening in all the studied temperatures (Figure 6, bottom). In these curves, it is specially worth mentioning the S-shaped curves observed at the highest measured temperatures (4-5 K), where a large positive slope at almost zero applied fields (H_{dc} < 0.1 T) is followed by a lower slope at higher fields. This shape, quite smoothed in the present case due to the weak magnetic interactions operating (*vide infra*), is indicative of a change in the regime of the magnetic ordering, in line with canted ferromagnetic behaviour. Furthermore, at 2 K remnant magnetization and coercive field values of 0.06 μ_B and 315 Oe were measured, respectively. According to equation 2, a small canting angle of 1.44° was estimated (M_R and M_S stand for remnant and saturation magnetization values, respectively):

$$\Psi = \tan^{-1}\left(\frac{M_R}{M_S}\right) \qquad (2)$$

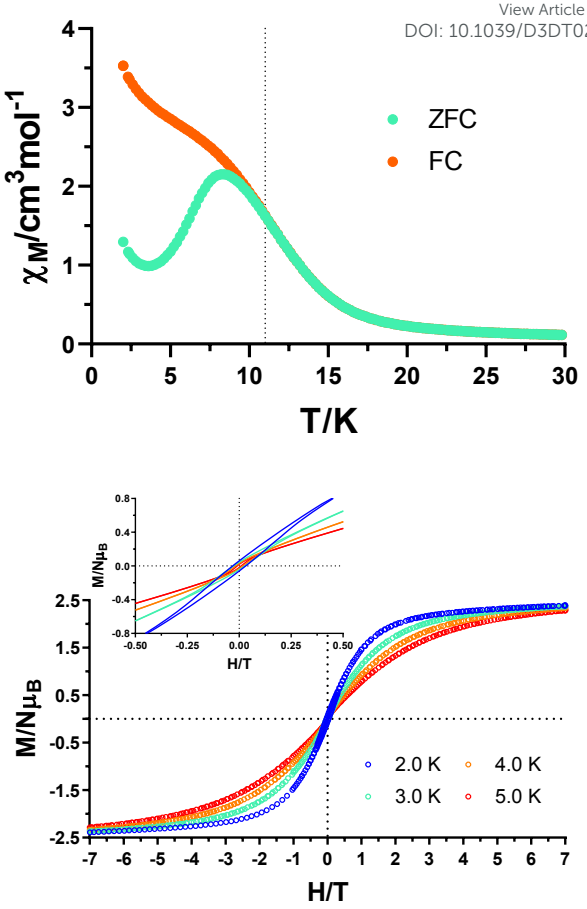

Figure 6. For **2**, temperature-dependent ZFC and FC molar susceptibility curves in the low temperature region (top) and magnetic hysteresis loops recorded in the 2-5 K temperature range (bottom).

Considering that complex **2** does not crystallize in a non-centrosymmetric space group, we assume that the spin-canting behaviour arises from the single-ion magnetic anisotropy of Co(II) ions and the relative dispositions between adjacent complexes in the structure forced by intermolecular Co···Co interactions, although there could be some superexchange pathway allowing for substantial antisymmetric exchange. In particular, the present structure is characterized by multiple intermolecular pathways along the spin carriers (take into account that intermolecular pathways in Figure 3 represent all potential magnetic couplings), all of which are expected to give very weak exchange interactions. Note, in this sense, that no reliable calculations could be performed to provide the magnitude of the exchange coupling through the exchange pathways owing to the limitations of DFT to estimate the value of *J* constant in these kind of superexchange pathways.[60] In principle, the strongest magnetic interaction should come from the so-called intralayer centrosymmetric pathway occurring through the π···π stacking between bq ligands because i) it brings the shortest Co···Co intermolecular distance (7.2 Å) in the structure and ii) the spin density is relatively large over the bq ligand (Figure S5). As reported in the latter works, ***π-π*** interactions are known to yield weak ferromagnetic couplings,[61,62] which seems to be the case of the present compound in view of the structural characteristics of the interacting bq ligands (see Table S6) Assuming that this interaction is

View Article Online
DOI: 10.1039/D3DT03759A

the strongest one along the 2D planes (drawn in red and green in Figure 3), there would be a net ferromagnetic ordering in the layers given the weaker superexchange couplings occurring through the remaining bridges within the layers. Hereafter, assuming that weak antiferromagnetic interactions may occur along the interlayer non-symmetric pathways (involving Co···Co of ca. 11 Å, see bottom of Figure 3), the magnetic moment of the 2D layers should not be fully cancelled with each other when packed along the crystallographic *b* axis. In fact, a representation of the *D*-tensor frame in two Co centres interacting through this large pathway shows how magnetic axes are not fully parallel, but canted to each other and thus, given the absence of symmetry elements different from *n* glide planes, uncompensated magnetic moments along the packing direction (*b* axis) lead to the observed spin-canting behavior (Figure S9). Taking into account that this explanation cannot be fully supported by calculations (in view of the impossibility to reliably calculate *J* constants), another possible explanation would suppose that interactions along the interlayer non-symmetric pathways are the main superexchange bridges governing the magnetic properties (canting the spins between individual complexes at low temperature), which is a priori more difficult to understand in view of the long Co···Co distances and low spin density present over the interacting atoms. In any case, the presence of the observed canting (involving S-shaped hysteresis curves) is well explained according to these two exchange pathways containing Co ions related by *n* glide planes, in which antisymmetric exchange could be non-zero. As an illustrative example, we would like to cite the research work reported by Zhang et al., in which they compare several one-dimensional Co(II) based compounds.[63] As they state, the coordination spheres in all compounds are comparable, as well as the intrachain magnetic interactions. However, different hydrogen-bond mediated Co···Co distances are responsible for activating/deactivating magnetic ordering in addition to the occurrence of SCM (Single-chain magnet) behaviour.

Taking into account that the long-range magnetic ordering prevents us from fitting the dc magnetic data of complex **2** and estimating the *zfs* parameters, theoretical calculations were essential in their evaluation. In this case, the calculation gives a large negative D = -59.4 cm^{-1} with also a large rhombicity of parameter(E/D = 0.21), which makes the sign of the main *D* parameter meaningless (see Table S7) as discussed before for compound **1**.[55–57] In order to understand the origin of the *zfs* parameters in this compound, we inspected the electronic configurations for the active space of the ground and lowest-lying states (see Table S10). As expected for a severely distorted square pyramid, all d-orbitals are separated in energy and the $(d_{yz})^2(d_{xz})^2(d_{xy})^1(d_{z^2})^1(d_{x^2-y^2})^1$ configuration is which better represents the ground state according to *ab initio* ligand field theory (AILFT) method (Figure 7). It is worth noting that d_{xy} and d_{xz} orbitals cannot be distinguished and appear to be admixed between HOMO and LUMO orbitals as a consequence of the large distortion present (Table S9), which could explain the sign of the lowest-lying transitions involved in the *zfs* parameters of the compound. As observed in Table S7, computational calculations predict negative and positive signs for the first and second excitations, which mainly represent the sign and magnitude of the *D* parameter. Therefore, according to the different $|m_l|$ value of d_{xy} (±2) and d_{xz}/d_{yz} (±1) orbitals and the transition energies (Table S10), a main $d_{xz} \rightarrow d_{xy}$ should govern the first transition whereas the second one should mainly consist of $d_{yz} \rightarrow d_{xz}$ (taking into account the minor, but still significant contribution of d_{xz} to the third orbital) transition, which can be only explained according to the previous admixture. Moreover, such admixture involving d_{xy} and d_{xz} orbitals, with a predominant equatorial and axial component, respectively, could also be the origin of the large rhombicity present in the compound and the ambiguous overall sign of the *zfs*.

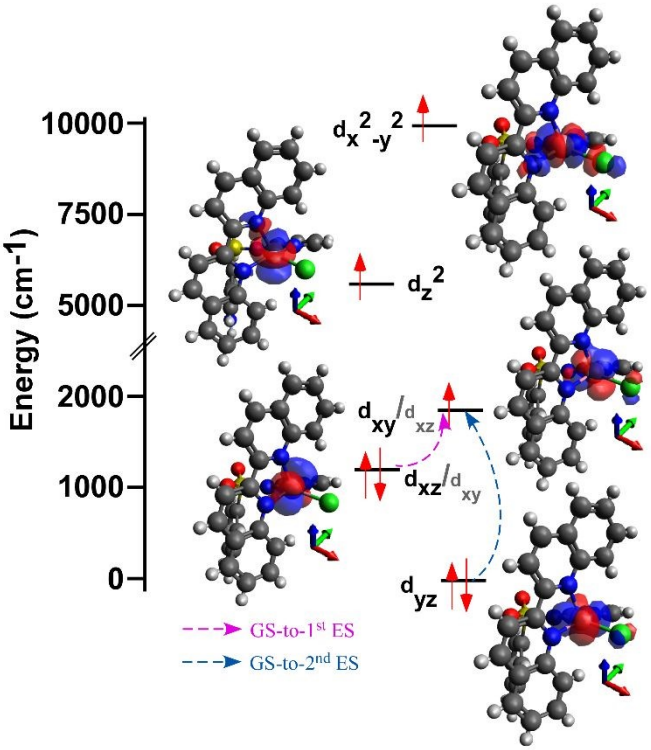

Figure 7. NEVPT2-AILFT computed d-orbital splitting for compound **2**. Dashed lines represent the first and second excitations which contribute to the *zfs* of the compound.

In spite of the significant magnetic anisotropy present, the occurrence of zero-field SMM behaviour is not expected in the present case in view of the large value for the matrix element (0.5 μ_B) connecting both ground Kramers doublets (Figure S11), which suggests that a considerable tunnelling effect could completely quench the slow magnetic relaxation. In addition, the possible SIM behaviour in this compound would compete with the long range magnetic ordering provided by spin-canting, which is the reason of subsequent dilution attempts.

As it will be described in the upcoming sections, the Ni(II) based counterpart **3** was synthesized in order to simulate a diamagnetic dilution of **2**, because it was not possible to synthesize the isostructural Zn(II) counterpart. This unconventional strategy is based in a recently published work reported by Zadrozny and coworkers,[64] where they took advantage of the positive *D* value of the Ni(II) counterpart in $(Ph_4P)_2[M(SPh)_4]$ (where M is Mn(II), Fe(II), Co(II) or Ni(II) in their study) that simulates a diamagnetic ground state (M_S = 0). Due to the lower expected magnetic anisotropy, the

$\chi_M T$ curve of **3** does not show any canted antiferromagnetism (Figure S12). In fact, this curve can be properly fitted with the PHI software by using the following Hamiltonian:

$$\hat{H} = \boldsymbol{D}\left(\hat{S}_z^2 - \boldsymbol{S}(\boldsymbol{S}+\boldsymbol{1})/\boldsymbol{3}\right) + \boldsymbol{\mu_B H g}\hat{S} - \boldsymbol{zJ'}\langle \boldsymbol{S_z}\rangle \boldsymbol{S_z} \qquad (3)$$

As observed in Figure S12, the susceptibility curve fits well to both positive and negative *D* values. In a first attempt, the curve was properly fitted affording D = +12.5(2) cm^{-1}, g = 2.2(0) and R = 2.2·10^{-2}, but without including the intermolecular -zJ interactions. In the second attempt, we obtained a similar result with the following set of parameters: D = -12.4(9) cm^{-1}, g = 2.3(0) and R = 7.1·10^{-2}, including a zJ = -0.5 cm^{-1}. The origin of such ambiguity is also explained according to the large rhombicity present in the compound as suggested by CAS-SCF/NEVPT2 calculations (vide infra, see Table S8). Considering the short M···M distances found in the crystal structure, and that intermolecular interactions govern the static and dynamic (*vide infra*) properties of the Co(II) based counterpart, both fitting procedures seem reasonable and, therefore, the ground state of **3** could be either M_S = ±1 or M_S = 0. Accordingly, the Ni/Co heterometallic mixture was studied to explore the possible improvement of SMM behaviour by means of the dilution of Co in Ni based matrix.

Dynamic magnetic properties

In view of the results provided by the theoretical calculations, which show large magnetic anisotropy in both compounds, dynamic ac magnetic measurements were carried out on both complexes at zero and optimal applied external magnetic dc fields in order to explore their SMM behaviour.

At zero applied dc field, no signal was observed in the $\chi''_M(T)$ plot for **1**, which may be due to the existence of a fast QTM process hiding the desired SMM behaviour (Figure S13). In view of that, field-dependence ac response was studied at 2 K. As observed in Figures S10-S11 SMM behaviour arises even at the lowest applied dc field of 250 Oe. Noteworthy, the slowest relaxation time was found at 1 kOe, being faster at 2.5 kOe due to the enhancement of a field-induced direct process. Thus, temperature- and frequency-dependent measurements were carried out with an external field of 1 kOe (Figure 7). In these conditions, QTM is at least partially quenched and **1** displays temperature- and frequency-dependent maxima below 4 K. Both $\chi''_M(\chi'_M)$ or Cole-Cole plots and $\chi''_M(v)$ curves were fitted to the generalized Debye model within in the 2-4 K temperature range (Figures S17-S18). As expected for an octahedral Co(II) complex, relaxation of the magnetization is best described by a Raman process (Figure 7, inset) instead of an Orbach mechanism involving excited states. In fact, a linear fit of the Arrhenius plot involves an U_{eff} = 9.2(2) K (6.4 cm^{-1}), a value that is much lower than the calculated 2D or the theoretically calculated energy gap between the ground and excited Kramers doublets by means of SINGLE_ANISO (244 K, 169.5 cm^{-1}, see Figure S10). In fact, a single Raman mechanism describes well the temperature dependence of the relaxation times, in agreement with the low α values calculated from the Cole-Cole plots (Figure S17). Thus, the temperature-dependence of the relaxation times was fitted to the following equation 4:

$$\tau^{-1} = BT^n \qquad (4)$$

The best fit provided B and n values of 2055(67) s^{-1}·K^{-n} and 2.36(2), respectively. Additionally, the lack of zero-field SMM behaviour is also well explained by the matrix element within the ground state, which predicts a large tunnelling phenomenon with a value of 1.7 μ_B (see Figure S10).

In good agreement with the long-range weak ferromagnetic ordering present in **2**, the data collected at zero-field showed temperature- and frequency-independent maxima both of the $\chi'_M(T)$ and $\chi''_M(T)$ signals (Figure S19 and Figure 8, middle). The fact of having these maxima at 11 K is in good agreement with the bifurcation temperature found in the FC/ZFC measurement. In order to confirm that the maxima do not correspond to SMM behaviour, the Mydosh parameter,[65] ϕ, was calculated using the formula $\phi = (\Delta T_P/T_P)/\Delta \log f$) and giving a value of ϕ = 0.04, which is consistent with a glassy state probably derived from the opposed weak ferro/antiferromagnetic interactions and not SMM behaviour.

Without discarding the possibility of a hidden SMM behaviour, field-dependent measurements were performed at 2.8 K for **2**. As depicted in Figures S20-S21, an optimum field of 1 kOe was determined for complex **2**. Under these optimal conditions, frequency-dependent maxima were measured below 6 K within $\chi''_M(T)$ plots in agreement with a field-induced SMM behaviour. Cole-Cole and $\chi''_M(v)$ plots were fitted within the 3.0-5.8 K temperature range and, once again, relaxation times were fitted to a Raman mechanism. The fitting to equation 4 provided B and n values of 0.58(2) s^{-1}·K^{-n} and 6.58(2), respectively. However, taking into account that the α values extracted from the Cole-Cole plots are slightly larger than those calculated for **1** (Figure S23), and considering the calculated D value, we also considered the simultaneous occurrence of Orbach and Raman mechanisms by equation 5:

$$\tau^{-1} = \tau_0^{-1} exp(-U_{eff}/K_BT) + BT^n \qquad (5)$$

Unfortunately, reasonable fitting parameters were not obtained. Before totally discarding the Orbach mechanism, we tried other attempts involving both QTM and direct processes along the Orbach relaxation pathway, but all our attempts were unsuccessful.

View Article Online
DOI: 10.1039/D2DT03594

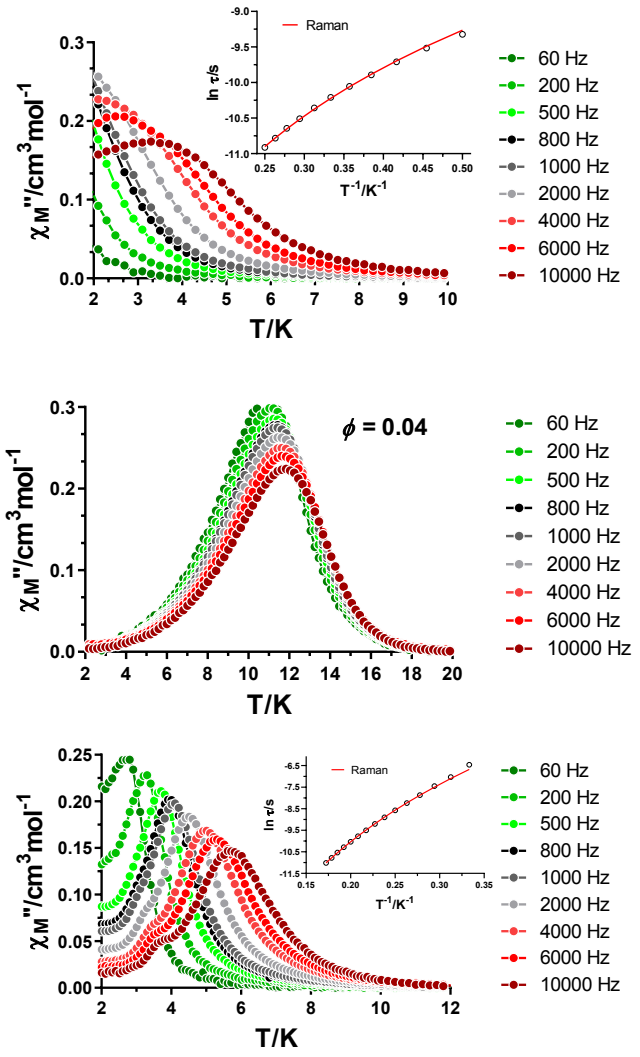

Figure 8. Temperature dependence of the out-of-phase components of the ac susceptibility in a dc applied field of 1 kOe for **1** (top) and **2** (bottom) and in a zero applied dc field for **2** (middle). Insets: Arrhenius plot for the relaxation times considering a Raman mechanism (top and bottom).

In view of the non-negligible Co···Co interactions appearing in **2**, we made several attempts in order to obtain the isostructural and diamagnetic Zn(II) counterpart to study the relaxation behaviour of a single [Co(SDZ)(bq)Cl] molecule in a diluted Zn-based matrix. However, no attempts involving $ZnCl_2$ afforded the desired compound. As an alternative route, we synthesized the Ni(II) counterpart **3**. Very recently, Zadrozny and coauthors have reported the relaxation dynamics of the $(Ph_4P)_2[Co(SPh)_4]$ zero-field SMM diluted in different paramagnetic matrices. As they show, when the SMM is diluted in a Ni(II) matrix with $D > 0$, the $M_S = 0$ sublevel is the only populated one at low temperatures with no spin angular momentum, which simulates, somehow, a dilution in a diamagnetic matrix alternative to the use of Zn(II). In that case, the dilution favours that relaxation times become slower due to an effective quenching of QTM.

In our work, we have tried to mimic their strategy for our compound **2**. Hence, compound $\mathbf{2_{Ni}}$ was successfully synthesized by using a 1:10 Co:Ni ratio showing purity and homogeneity by PXRD analysis (Figure S2). Once again, dynamic ac magnetic measurements were initially studied under zero applied dc field. Considering that **3** does not show any measurable spin-canted effect in the $\chi_M T$ curve, we did not expect it within $\mathbf{2_{Ni}}$. However, as clearly observed in Figures S25-S26, this diluted analogue displays frequency-independent maxima at 6.5 K in agreement with the long-range magnetic ordering shown by the cobalt analogue. In view of that, and with the aim of comparing the relaxation times measured in the same experimental conditions, ac magnetic properties of $\mathbf{2_{Ni}}$ were studied under an external magnetic dc field of 1 kOe. The $\chi''_M(T)$ plots reveal field-induced SMM behaviour with maxima below 5.2 K, a slightly lower temperature than for **2** (Figure S28). Relaxation times and α values were obtained by fitting the Cole-Cole and $\chi''_M(\nu)$ plots in the 2.0-5.2 K temperature range. As observed in Figure 9, relaxation times for $\mathbf{2_{Ni}}$ display a larger curvature than that expected for a single Raman mechanism (dashed blue line). This is supported by the slightly larger α values obtained for this compound, which suggest the occurrence of an additional magnetic relaxation pathway. Thus, we considered the simultaneous presence of a Raman and direct process by the following equation:

$$\tau^{-1} = BT^n + A_{direct}T \qquad (6)$$

The fit afforded the following set of parameters: $B = 27(6)\ s^{-1}\cdot K^{-n}$; $n = 4.4(1)$ and $A_{direct} = 1881(120)\ s^{-1}\cdot K^{-1}$. Note that a similar fit could be obtained by replacing the direct mechanism with QTM (Figure S31). In any case, the most important conclusion is that relaxation times are faster for $\mathbf{2_{Ni}}$ than for **2** in the whole temperature regime.

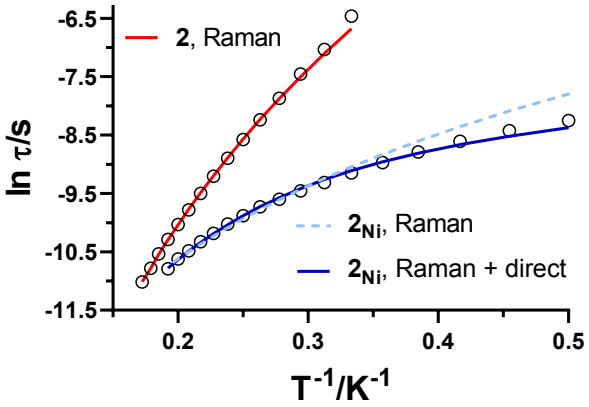

Figure 9. Comparison of the Arrhenius plots for the relaxation times obtained for compounds **2** (red) and $\mathbf{2_{Ni}}$ (blue) measured at the same experimental conditions.

It is clear that this system is not appropriate to perform the mentioned approach. Indeed, in view of the evolution of the relaxation times, we assume that the Ni(II) based counterpart must have a non-desired negative D value with $M_S = \pm 1$ as ground state. *Ab initio* calculations based on an optimized nickel-based model give $D = -21.5\ cm^{-1}$ although the negative sign is, again, not meaningful in view of the large rhombicity ($E/D = 0.22$, see Table S8). Consequently, these results could explain why the relaxation times are not slowed down in this case because, although those few [Co(SDZ)(bq)Cl] complexes were aimed to be surrounded by either completely diamagnetic (with Zn(II)) or somehow, diamagnetic ions at low temperatures (Ni(II) with $D > 0$), they possess neighbouring paramagnetic molecules. In this sense, it is worth mentioning that the system that we have studied in this work and $(Ph_4P)_2[Co(SPh)_4]$

display notable differences. On the one hand, in the previously reported case, the paramagnetic centres within the crystal structure are much farther from each other and no sizeable interaction is observed. In our case, instead, the short Co···Co distances appeared to be fundamental when explaining the magnetic properties. On the other hand, $(Ph_4P)_2[Co(SPh)_4]$ behaves as zero-field SMM while in our case an external magnetic field needs to be applied to observe slow relaxation of the magnetization.

Conclusions

We have successfully synthesized and characterized two novel Co(II) based mononuclear compounds based on SDZ and additional chelating phen and bq ligands named as **1** (phen) and **2** (bq). Moreover, the isostructural Ni(II) analogue of **2** has been prepared for further magnetic studies. As predicted, the coordination sphere differs from one to another due to the bulky character of bq, having a CoN_6 and CoN_4Cl spheres for **1** and **2**, respectively. Consequently, both compounds share sizeable magnetic anisotropy characterized by significant rhombicity as suggested by experimental magnetic studies and theoretical calculations. The negative (although meaningless) sign of the calculated *D* parameter in **2** is probably due to an admixture involving d_{xy} and d_{xz} orbitals, which could also be the origin of the large rhombicity present in the compound. As reported for other octahedral Co(II) based magnets, **1** behaves as field-induced SMM with a magnetization relaxation mechanism based on a Raman process. In contrast, complex **2** displays a spin-canted antiferromagnetism that, perhaps, hides slow magnetic relaxation at zero applied dc field. Under an optimal external magnetic field, field-induced SMM behaviour arises with a relaxation process governed by a Raman mechanism. In view of the unsuccessful preparation of the Zn(II) counterpart of **2**, [Co(SDZ)(bq)Cl] was diluted in a Ni(II) matrix yielding compound $\mathbf{2_{Ni}}$. This new compound still displays spin-canted antiferromagnetism and, therefore, the potential zero-field SMM behaviour did not emerge in this material. Besides, relaxation rates occur to be even faster than the pure compound **2**, evidencing a paramagnetic ground-state for the Ni(II) counterpart, also demonstrated by theoretical calculations. Further work is in progress to study other paramagnetic dilutions with the aim of understanding the differences that might appear by carrying out dilutions with other metal ions. Moreover, solution studies of **2** would be also interesting in order to confirm or deny the potential zero-field SMM behaviour of [Co(SDZ)(bq)Cl].

Conflicts of interest

There are no conflicts to declare.

Acknowledgements

C.V-P acknowledges the financial support from ANPCYT (PICT 2019-02589). D.B.S and G.R would like to thank to Universidad Nacional de La Plata (UNLP) 11X/876 and X857 and CONICET. The financial support by Gobierno Vasco/Eusko Jaurlaritza (IT1755-22) is also acknowledged. The authors thank for technical and human support provided by the Geochronology and Isotope Geochemistry-SGIker facility of UPV/EHU and European funding (ERDF and ESF). The authors acknowledge Dr. María Mar Quesada-Moreno for insightful discussions and help with the quantum-chemical calculations, and they are also grateful to Dr. Oscar Castillo for the enlightening discussions about magnetic properties of these compounds.

References

1 R. Sessoli, D. Gatteschi, A. Caneschi and M. A. Novak, *Nature*, 1993, **365**, 141–143.
2 F. Neese and D. A. Pantazis, *Faraday Discuss.*, 2011, 148, 229–238.
3 N. Ishikawa, M. Sugita, T. Ishikawa, S. Y. Koshihara and Y. Kaizu, *J. Am. Chem. Soc.*, 2003, **125**, 8694–8695.
4 A. Zabala-Lekuona, J. M. Seco and E. Colacio, *Coord. Chem. Rev.*, 2021, **441**, 213984.
5 J. Su, L. Yin, Z. Ouyang, Z. Wang and W. Zheng, *Dalt. Trans.*, 2020, **49**, 6945–6949.
6 A. Cornia, A. L. Barra, V. Bulicanu, R. Clérac, M. Cortijo, E. A. Hillard, R. Galavotti, A. Lunghi, A. Nicolini, M. Rouzières, L. Sorace and F. Totti, *Inorg. Chem.*, 2020, **59**, 1763–1777.
7 N. I. Gumerova, A. Roller, G. Giester, J. Krzystek, J. Cano and A. Rompel, *J. Am. Chem. Soc.*, 2020, **142**, 3336–3339.
8 R. C. Poulten, M. J. Page, A. G. Algarra, J. J. Le Roy, I. López, E. Carter, A. Llobet, S. A. Macgregor, M. F. Mahon, D. M. Murphy, M. Murugesu and M. K. Whittlesey, *J. Am. Chem. Soc.*, 2013, **135**, 13640–13643.
9 J. Miklovič, D. Valigura, R. Boča and J. Titiš, *Dalt. Trans.*, 2015, **44**, 12484–12487.
10 K. E. R. Marriott, L. Bhaskaran, C. Wilson, M. Medarde, S. T. Ochsenbein, S. Hill and M. Murrie, *Chem. Sci.*, 2015, **6**, 6823–6828.
11 J. M. Zadrozny, D. J. Xiao, M. Atanasov, G. J. Long, F. Grandjean, F. Neese and J. R. Long, *Nat. Chem.*, 2013, **5**, 577–581.
12 J. M. Zadrozny, M. Atanasov, A. M. Bryan, C. Y. Lin, B. D. Rekken, P. P. Power, F. Neese and J. R. Long, *Chem. Sci.*, 2013, **4**, 125–138.
13 J. M. Zadrozny and J. R. Long, *J. Am. Chem. Soc.*, 2011, **133**, 20732–20734.
14 T. Jurca, A. Farghal, P. H. Lin, I. Korobkov, M. Murugesu and D. S. Richeson, *J. Am. Chem. Soc.*, 2011, **133**, 15814–15817.
15 J. Vallejo, A. Pascual-Álvarez, J. Cano, I. Castro, M. Julve, F. Lloret, J. Krzystek, G. De Munno, D. Armentano, W. Wernsdorfer, R. Ruiz-García and E. Pardo, *Angew. Chemie - Int. Ed.*, 2013, **52**, 14075–14079.
16 R. Ishikawa, R. Miyamoto, H. Nojiri, B. K. Breedlove and M. Yamashita, *Inorg. Chem.*, 2013, **52**, 8300–8302.
17 X. N. Yao, J. Z. Du, Y. Q. Zhang, X. B. Leng, M. W. Yang, S. Da Jiang, Z. X. Wang, Z. W. Ouyang, L. Deng, B. W. Wang and S. Gao, *J. Am. Chem. Soc.*, 2017, **139**, 373–380.
18 P. C. Bunting, M. Atanasov, E. Damgaard-Møller, M. Perfetti, I. Crassee, M. Orlita, J. Overgaard, J. Van Slageren,

View Article Online
DOI: 10.1039/D3DT02359A

F. Neese and J. R. Long, *Science (80-.).*, 2018, **362**, 7319.
19 J. M. Frost, K. L. M. Harriman and M. Murugesu, *Chem. Sci.*, 2016, **7**, 2470–2491.
20 G. A. Craig and M. Murrie, *Chem. Soc. Rev.*, 2015, **44**, 2135–2147.
21 Y. F. Deng, T. Han, Z. Wang, Z. Ouyang, B. Yin, Z. Zheng, J. Krzystek and Y. Z. Zheng, *Chem. Commun.*, 2015, **51**, 17688–17691.
22 C. Villa-Pérez, I. Oyarzabal, G. A. Echeverría, G. C. Valencia-Uribe, J. M. Seco and D. B. Soria, *Eur. J. Inorg. Chem.*, 2016, **2016**, 4835–4841.
23 M. Feng and M. L. Tong, *Chem. - A Eur. J.*, 2018, **24**, 7574–7594.
24 X. X. Jin, X. X. Chen, J. Xiang, Y. Z. Chen, L. H. Jia, B. W. Wang, S. C. Cheng, X. Zhou, C. F. Leung and S. Gao, *Inorg. Chem.*, 2018, **57**, 3761–3774.
25 L. Chen, J. Wang, J.-M. Wei, W. Wersndorfer, X.-T. Chen, Y.-Q. Zhang, Y. Song and Z.-L. Xue, *J. Am. Chem. Soc.*, 2014, **136**, 12213–12216.
26 L. Chen, S. Y. Chen, Y. C. Sun, Y. M. Guo, L. Yu, X. T. Chen, Z. Wang, Z. W. Ouyang, Y. Song and Z. L. Xue, *Dalt. Trans.*, 2015, **44**, 11482–11490.
27 A. Sarkar, S. Dey and G. Rajaraman, *Chem. - A Eur. J.*, 2020, **26**, 14036–14058.
28 J. B. Tommasino, F. N. R. Renaud, D. Luneau and G. Pilet, *Polyhedron*, 2011, **30**, 1663–1670.
29 O. Pajuelo-Corral, A. Zabala-Lekuona, E. San Sebastian, A. Rodríguez-Diéguez, J. A. García, L. Lezama, E. Colacio, J. M. Seco and J. Cepeda, *Chem. – A Eur. J.*, 2020, **26**, 13484–13498.
30 S. Titos-Padilla, J. Ruiz, J. M. Herrera, E. K. Brechin, W. Wersndorfer, F. Lloret and E. Colacio, *Inorg. Chem.*, 2013, **52**, 9620–9626.
31 S. G. de Madinabeitia, M. E. S. Lorda and J. I. G. Ibarguchi, *Anal. Chim. Acta*, 2008, **625**, 117–130.
32 CrysAlis CCD (Computer Software), *CrysAlis RED and associated programs: Oxford Diffraction program.*, Oxford Diffraction Ltd, Abingdon, England, 2006.
33 G. M. Sheldrick, *SHELXS-97. Program for Crystal Structure Resolution.*, University of Göttingem, Göttingen, Germany, 1997.
34 G. M. Sheldrick, *SHELXL-97. Program for Crystal Structure Analysis.*, University of Göttingem, Göttingen, Germany, 1997.
35 M. J. Frisch, G. W. Trucks, H. B. Schlegel, G. E. Scuseria, M. A. Robb, J. R. Cheeseman, G. Scalmani, V. Barone, G. A. Petersson, H. Nakatsuji, X. Li, M. Caricato, A. V Marenich, J. Bloino, B. G. Janesko, R. Gomperts, B. Mennucci, H. P. Hratchian, J. V Ortiz, A. F. Izmaylov, J. L. Sonnenberg, D. Williams-Young, F. Ding, F. Lipparini, F. Egidi, J. Goings, B. Peng, A. Petrone, T. Henderson, D. Ranasinghe, V. G. Zakrzewski, J. Gao, N. Rega, G. Zheng, W. Liang, M. Hada, M. Ehara, K. Toyota, R. Fukuda, J. Hasegawa, M. Ishida, T. Nakajima, Y. Honda, O. Kitao, H. Nakai, T. Vreven, K. Throssell, J. A. Montgomery Jr., J. E. Peralta, F. Ogliaro, M. J. Bearpark, J. J. Heyd, E. N. Brothers, K. N. Kudin, V. N. Staroverov, T. A. Keith, R. Kobayashi, J. Normand, K. Raghavachari, A. P. Rendell, J. C. Burant, S. S. Iyengar, J. Tomasi, M. Cossi, J. M. Millam, M. Klene, C. Adamo, R. Cammi, J. W. Ochterski, R. L. Martin, K. Morokuma, O. Farkas, J. B. Foresman and D. J. Fox, 2016.
36 A. D. Becke, *Phys. Rev. A*, 1988, **38**, 3098–3100.
37 A. Schäfer, H. Horn and R. Ahlrichs, *J. Chem. Phys.*, 1992, **97**, 2571–2577.
38 V. A. Rassolov, J. A. Pople, M. A. Ratner and T. L. Windus, *J. Chem. Phys.*, 1998, **109**, 1223–1229.
39 F. Neese, F. Wennmohs, U. Becker and C. Riplinger, *J. Chem. Phys.*, 2020, **152**, 224108.
40 F. Neese, *WIREs Comput. Mol. Sci.*, 2012, **2**, 73–78.
41 C. Lee, W. Yang and R. G. Parr, *Phys. Rev. B*, 1988, **37**, 785–789.
42 A. D. Becke, *J. Chem. Phys.*, 1993, **98**, 5648–5652.
43 C. van Wüllen, *J. Chem. Phys.*, 1998, **109**, 392–399.
44 F. Weigend and R. Ahlrichs, *Phys. Chem. Chem. Phys.*, 2005, **7**, 3297–3305.
45 F. Weigend, *Phys. Chem. Chem. Phys.*, 2006, **8**, 1057–1065.
46 A. Hellweg, C. Hättig, S. Höfener and W. Klopper, *Theor. Chem. Acc.*, 2007, **117**, 587–597.
47 Y. F. Deng, M. K. Singh, D. Gan, T. Xiao, Y. Wang, S. Liu, Z. Wang, Z. Ouyang, Y. Z. Zhang and K. R. Dunbar, *Inorg. Chem.*, 2020, **59**, 7622–7630.
48 C. Angeli, S. Borini, M. Cestari and R. Cimiraglia, *J. Chem. Phys.*, 2004, **121**, 4043–4049.
49 D. Maganas, S. Sottini, P. Kyritsis, E. J. J. Groenen and F. Neese, *Inorg. Chem.*, 2011, **50**, 8741–8754.
50 M. Llunell, D. Casanova, J. Cirera, J. M. Bofill, P. Alemany, S. Alvarez, M. Pinsky and D. Avnir, *SHAPE (Computer Software)*, Barcelona, 2005.
51 J. E. Campbell, J. Yang and G. M. Day, *J. Mater. Chem. C*, 2017, **5**, 7574–7584.
52 A. Guijarro, J. A. Vergés, E. San-Fabián, G. Chiappe and E. Louis, *ChemPhysChem*, 2016, **17**, 3548–3557.
53 R. Boča, C. Rajnák and J. Titiš, *Magnetochemistry 2023, Vol. 9, Page 100*, 2023, **9**, 100.
54 N. F. Chilton, R. P. Anderson, L. D. Turner, A. Soncini and K. S. Murray, *J. Comput. Chem.*, 2013, **34**, 1164–1175.
55 M. Atanasov, D. Aravena, E. Suturina, E. Bill, D. Maganas and F. Neese, *Coord. Chem. Rev.*, 2015, **289–290**, 177–214.
56 J. Cirera, E. Ruiz, S. Alvarez, F. Neese and J. Kortus, *Chem. - A Eur. J.*, 2009, **15**, 4078–4087.
57 D. Maganas, J. Krzystek, E. Ferentinos, A. M. Whyte, N. Robertson, V. Psycharis, A. Terzis, F. Neese and P. Kyritsis, *Inorg. Chem.*, 2012, **51**, 7218–7231.
58 R. Herchel, L. Váhovská, I. Potočňák and Z. Trávníček, *Inorg. Chem.*, 2014, **53**, 5896–5898.
59 E. Colacio, J. Ruiz, E. Ruiz, E. Cremades, J. Krzystek, S. Carretta, J. Cano, T. Guidi, W. Wernsdorfer and E. K. Brechin, *Angew. Chemie Int. Ed.*, 2013, **52**, 9130–9134.
60 M. Fumanal, J. Jornet-Somoza, S. Vela, J. J. Novoa, J. Ribas-Arino and M. Deumal, *J. Mater. Chem. C*, 2021, **9**, 10647–10660.
61 Y. H. Chi, L. Yu, J. M. Shi, Y. Q. Zhang, T. Q. Hu, G. Q. Zhang, W. Shi and P. Cheng, *Dalt. Trans.*, 2011, **40**, 1453–1462.
62 C. Hou, J. M. Shi, Y. M. Sun, W. Shi, P. Cheng and L. D. Liu,

View Article Online
DOI: 10.1039/D3DT02359A

Dalt. Trans., 2008, 5970–5976.

63 Y. Zhang, Z. Y. Liu, H. M. Tang, B. Ding, Z. Y. Liu, X. G. Wang, X. J. Zhao and E. C. Yang, *Inorg. Chem. Front.*, 2022, **9**, 5039–5047.

64 I. P. Moseley, C. P. Ard, J. A. DiVerdi, A. Ozarowski, H. Chen and J. M. Zadrozny, *Cell Reports Phys. Sci.*, 2022, **3**, 100802.

65 J. A. Mydosh, *Spin Glasses*, Taylor & Francis: Washington, DC, 1993.